# Gas-Permeable, Ultrathin, Stretchable Epidermal

## Electronics with Porous Electrodes

Weixin Zhou, †‡ Shanshan Yao, ‡§ Hongyu Wang, ‡ Qingchuan Du, † Yanwen Ma, †\* Yong Zhu‡\*

† Institute of Advanced Materials, Nanjing University of Posts and Telecommunications,

Nanjing, Jiangsu 210023, China

<sup>‡</sup>Department of Mechanical and Aerospace Engineering, North Carolina State University,

Raleigh, NC 27695-7910, USA

§Present Address: Department of Mechanical Engineering, Stony Brook University, Stony

Brook, NY 11794-2300, USA

## **Corresponding Authors**

\*E-mail: yong zhu@ncsu.edu or iamywma@njupt.edu.cn

## **ABSTRACT**

We present gas-permeable, ultrathin, and stretchable electrodes enabled by self-assembled porous substrates and conductive nanostructures. Efficient and scalable breath figure method is employed to introduce the porous skeleton and then silver nanowires (AgNWs) are dip-coated and heat-pressed to offer electric conductivity. The resulting film has a transmittance of 61%, sheet

resistance of 7.3  $\Omega$ /sq, and water vapor permeability of 23 mg cm<sup>-2</sup> h<sup>-1</sup>. With AgNWs embedded below the surface of the polymer, the electrode exhibits excellent stability with the presence of sweat and after long-term wear. We demonstrate the promising potential of the electrode for wearable electronics in two representative applications – skin-mountable biopotential sensing for healthcare and textile-integrated touch sensing for human-machine interfaces. The electrode can form conformal contact with human skin, leading to low skin-electrode impedance and high-quality biopotential signals. In addition, the textile electrode can be used in a self-capacitance wireless touch sensing system.

**KEYWORDS:** gas permeable; breath figure; silver nanowires; healthcare; human-machine interfaces

Epidermal electronics has seen a wide range of applications from personal healthcare to human activity monitoring to human-machine interfaces. <sup>1-12</sup> It is critical that epidermal electronics forms conformal contact with the skin in order to improve the quality of sensing signals. <sup>13-16</sup> Currently most epidermal devices are built on solid polymeric substrates, such as polydimethylsiloxane (PDMS), polyethylene terephthalate (PET), and polyimide (PI), which lack efficient gas permeability. <sup>17-20</sup> This can prevent evaporation of sweat and emission of volatile organic components from human skin, leading to skin irritation and reducing the comfort of wearing. Therefore, to achieve long-term wearing, it is imperative to develop gas permeable materials.

In order to improve gas permeability and achieve conformal contact, a number of architectures have been pursued in recent years, including textiles, meshes and porous structures. For example, Someya and co-workers recently reported an ultrathin nanomesh electrode with electrospun polyvinyl alcohol (PVA) film, which showed good gas permeability, but the fabrication process was rather complicated. Fan *et al.*, developed an electrospun PVA and silver nanowire (AgNWs) conductive composite, which increased the robustness in electrical stability, but the exposed nanowires limited the long-term stability. Another method employed sugar templates to prepare PDMS sponge and transfer a thin layer of graphene onto the surface of the sponge as the conductive material. Limited by the size of the sugar particles, this method was difficult to prepare micropore structures. In addition, this method was not feasible to fabricate ultrathin films. It remains challenging to develop gas-permeable and ultra-thin materials in a simple and scalable fashion.

Here we report a stretchable conductive film prepared by embedding AgNWs just below the surface of a porous thermoplastic polyurethane (TPU) film fabricated by breath figure method. Breath figure method is a simple, efficient and scalable self-assembly process to fabricate porous polymer films, <sup>21, 22</sup> no need for complex steps such as photolithography, vacuum evaporation, and

etching. Compared with other methods, such as stamping or imprinting, this method has the advantage of low-cost, one-step, and template-free fabrication. Moreover, the porous film has good gas permeability for sweat evaporation to prevent skin irritation. The ultra-thin nature of this film enables a conformal contact with the skin, which can improve the signal quality of the electrophysiological (EP) sensing as well as the long-term wearing comfort. Utility of the thin-film electrodes for epidermal electronics is demonstrated in skin-mountable electrodes for EP sensing and textile-integrated touch sensors for human-machine interfaces.

#### RESULTS AND DISCUSSION

A schematic illustration of the fabrication process is shown in Figure 1a. Briefly, a porous TPU film was prepared using a breath figure method, and AgNWs were dip-coated onto the surface. Heat press treatment was performed to melt the TPU surface and embed AgNWs just below its surface. In the breath figure process, tetrahydrofuran (THF) was used as the solvent. In addition, a small amount of polyethylene glycol (PEG) (TPU: PEG = 10:1 in weight) was added to the solution to facilitate the ordered assembly of water droplets.<sup>23</sup> Evaporation of the organic solvent cooled down the substrate. The moisture condensed on the substrate and self-assembled into regular water drop arrays. Typically the convergence of water droplets should be avoided, which otherwise could lead to disordered structures.<sup>21, 22</sup> However, in this work, the convergence of droplets contributed to the formation of through-pore structures. As shown in Figure 1b and Figure S1, the pore size can be controlled by changing the concentration of the solution. Higher concentration (2 wt% TPU + 0.2 wt% PEG) led to smaller pore size and more regular pore structure, but higher percentage of dead-end pores. On the other hand, when the concentration was too low (1 wt% TPU + 0.1 wt% PEG), the resulting structure tended to be more irregular with pore diameter larger than 100 µm.

Such large pores can become visible to naked eyes and pose a limit to the patterning resolution of the electrodes. The optimum solution concentration was found to be 1.5 wt% TPU and 0.15 wt% PEG. As can be seen from the optical and scanning electron microscope (SEM) images in Figure 1b and e, the porous structure was evenly distributed. The shape of the pores was close to circular with a pore diameter of  $\sim$ 40  $\mu$ m, and the pore coverage ratio is about 39%(Figure 1e, f).

AgNWs were loaded onto the porous TPU film by dipping the film into the AgNW/water solution. The pore size of the TPU film was much larger than the length of AgNWs ( $\sim$ 20  $\mu$ m). Figure 1c shows the optical and SEM images of the porous AgNW/TPU film, where AgNWs were uniformly coated on the surface of TPU without hanging across pores. Dip-coated AgNWs on the TPU surface were easy to detach from the film, so a heat press treatment was introduced to enhance the adhesion. Since the melting point of the TPU is around 130 °C, a temperature of 150 °C was used for heat pressing. It can be observed from Figure 1d2 that, after the heat press, majority of the AgNWs were inlaid inside TPU with only a small portion exposed on the surface. This morphology was further illustrated in the cross-sectional SEM images (Figure S2). The thickness of the porous AgNW/TPU film decreased from 6.8  $\mu$ m to 4.6  $\mu$ m after the heat press.

Figure 2a shows the optical image of the porous HP-AgNW/TPU film. Figure 2b shows the sheet resistance as a function of the number of dip-coating cycles. The sheet resistance decreased with coating cycles for the first 4 cycles. After that, the sheet resistance remained nearly constant with more coating cycles, reaching about 14.5  $\Omega$ /sq. Hence 4 cycles of dip coating were used in the fabrication. The heat press treatment further decreased the resistance, which can be attributed to the improved contact in the AgNW junctions caused by the pressure and thermal annealing during heat press. For example, after heat press the sheet resistance of 4-cycle-coated film decreased to 7.3  $\Omega$ /sq. The porous structure of the film led to enhanced optical transparence compared to the

solid film. The optical transmittance was 72% at 550 nm for the porous TPU film (Figure 2c) and decreased to 63% after dip-coating AgNWs for 4 cycles. The transmittance further decreased to 61% after the heat press, due to the slightly increased width of the TPU skeleton and thus reduced pore coverage ratio. To investigate the mechanical properties of these porous films, we tested the stress-strain curves of porous TPU, AgNW/TPU, and HP-AgNW/TPU films. As shown in Figure S3, the HP-AgNW/TPU film shows the highest stiffness, which is likely because the film became denser and the AgNWs formed stronger bonds with TPU and between themselves.

The water vapor transmission was evaluated based on the ASTM's E96 standard.<sup>26</sup> The porous TPU film exhibited dramatically enhanced vapor permeability compared to a TPU film without the porous structure (Figure 2d). The water vapor transmission rates of solid TPU, porous TPU, porous AgNW/TPU, and porous HP-AgNW/TPU were measured to be 2, 38, 36, and 23 mg cm<sup>2</sup> h<sup>-1</sup>, respectively. Enhanced vapor permeability was hypothesized to render better long-term wearability. To test the hypothesis, a long-term on-skin wearability test was carried out (Figure S4). After 7 days of wearing on human skin, no allergic reactions and sweat accumulation occurred. No difference was observed between the skin area that was covered by the film and the surrounding area. It is apparent that the through-pore structure allows sweat and moisture to escape through the film, reduces the likelihood of skin irritation, and improves the comfortableness and long-term wearability for wearable applications.

The films were immersed in a saline solution to demonstrate the long-term stability in sweat (Figure 2e). After 100 hours, the resistance of porous AgNW/TPU and HP-AgNW/TPU films increased by 60% and 15%, respectively. Peel tests were performed between the film and a tape (Figure 2f) and between the film and skin (Figure S5). Figure 2f shows that, the AgNW/TPU film can be easily peeled off by the tape (the image on the right shows the AgNWs transferred onto the

tape), while the HP-AgNW/TPU film is much more stable. In addition, the AgNW/TPU film lost the conductivity after the peeling test, while the HP-AgNW/TPU film maintained the conductivity. As shown in Figure S5, after peeling the AgNW/TPU film off the skin, some AgNWs were left on the skin. For the case of HP-Ag NW/TPU film, no obvious residue of AgNWs was observed on the skin. These experiments revealed that the heat press treatment can effectively improve the conductivity and stability for long-term wearable applications. By embedding AgNWs below the surface of TPU film, the resulting porous HP-AgNW/TPU film showed significantly enhanced adhesion between AgNWs and TPU and hence stability, with acceptable sacrifice of optical transmittance and vapor permeability.

It is worth noting that the HP-AgNW/TPU film is not only conductive on the surface but also in the thickness direction. The top and bottom sides of the film were both electrically conductive; both sides were also connected by AgNWs on the edge of the pores through the thickness. It works like a bulk conductive material but does not require a large amount of conductive fillers, which could cause degradation in the mechanical properties. To demonstrate this property, the film was connected to a LED circuit and used as a double-sided conductor (Figure S6). Two droplets of liquid metal were applied on the two sides of the film to interconnect with the LED. The lighted LED indicated that both sides of the film are electrically conductive and connected.

The porous HP-AgNW/TPU film can be laser-cut into different patterns. Figure 3a shows a film electrode patterned into a filamentary serpentine structure with linewidth of 0.5 mm. The electrode can be used for electrocardiography (ECG) and electromyography (EMG) (to be discussed later). The ultrathin nature of the film enabled intimate contact with the skin. By spraying a small amount of breathable liquid bandage (Nexcare<sup>TM</sup>, 3M) onto the skin, the film electrode can be easily laminated onto the skin (Movie S1). The film can be stretched, compressed, and twisted on skin

(Figure 3a) and completely recovered. After use, the film can be easily removed using a scotch tape (Movie S2) and re-used for many times. The efficient lamination and removal demonstrated excellent user-friendliness of the porous HP-AgNW/TPU electrode.

Figure 3b presents the change in resistance as a function of tensile strain. When 5% strain was applied to the porous HP-AgNW/TPU film, the resistance was doubled. When the strain was released to zero, the resistance had a slight drop of 10%. In the subsequent stretch-release cycles within the 5% strain, the resistance remained nearly constant and reversible. When stretched to 10% and 15% strains, the resistances increased about 4 and 7 times, respectively, compared to the initial value. But within the 10% and 15% strains, the similar trend to the 5% strain was seen: the resistance increased rapidly during the first stretch and then became reversible in the following stretch-release cycles with small resistance change. At each strain level, the film can be "programmed" by the first stretch, after which the resistance would change reversibly within the range defined by the first stretch.

This "programmed" phenomenon is attributed to plastic deformation and buckling of the HP-AgNW/TPU film. During the first stretching, sliding between AgNWs and the porous TPU film occurs, which results in the surface buckling upon release of the strain. When the applied strain is relatively small (*e.g.*, 5%), the surface buckling is the microstructural origin of the reversible change in the resistance.<sup>27-31</sup> Under larger applied strain (*e.g.*, 10% or 15%), TPU undergoes plastic deformation, leading to irreversible structural deformation. For example, as shown in Figure 3b, the permanent (plastic) strain was ~3% when unloaded from the 15% strain. Nevertheless, between 3% and 15% strains the resistance was totally reversible, due to the surface buckling mechanism. The measurement of resistance changes for 1,000 cycles of stretching (10%) and release is shown in Figure S7. After 1,000 cycles, the resistance increased less than 7%. In addition, the HP-

AgNW/TPU film exhibited excellent flexibility. When the film was bent to a curvature of 0.55 mm<sup>-1</sup>, the resistance only increased by 0.8% (Figure 3c). After 10,000 cycles of bending, the resistance increased by 0.7% (Figure 3d). Besides, the resistance change of the porous HP-AgNW / TPU film under large strain is shown in Figure S8. It can be seen that the film remains conductive until 45% strain. The breakage strain of the HP-AgNW / TPU film is about 350%.

The porous HP-AgNW/TPU film is well suited for continuous monitoring of electrophysiological signals. ECG is commonly used to diagnose abnormal heart rhythms, while EMG can be used to analyze stimulation levels, muscle neuropathy, and motor behavior. In ECG and EMG measurements, conformal contact and low skin-electrode impedance is crucial for obtaining high signal-to-noise ratio. <sup>13, 17</sup> To assess the contact between the porous HP-AgNW/TPU electrodes and the skin, artificial skin made of Exoflex was fabricated, which replicates the human skin with a similar Young's modulus. Figure 4a and Figure S9 show the optical images of the electrode after transferred onto the artificial skin. It can be seen that the ultrathin electrode formed a conformal contact with the skin. Figure 3a also shows conformal contact between the electrode and the skin.

The impedances for the original and stretched porous HP-AgNW/TPU electrodes were only slightly higher than that of the commercial Ag/AgCl gel electrodes (Figure 4d), and lower than that of the solid AgNW/PDMS film (thickness 0.2 mm), which was demonstrated previously.<sup>32</sup> The difference is related to the quality of the skin-electrode contact. The reduced thickness and the porous structure of the porous HP-AgNW/TPU film decrease the bending stiffness, leading to more conformal contact than the solid AgNW/PDMS film.

ECG and EMG signals obtained using the porous HP-AgNW/TPU electrodes were compared against those using the commercial Ag/AgCl gel electrodes, as shown in Figure 4e and f. Figure 4b and c show the placement of the electrodes for ECG and EMG testing, respectively. For ECG, the porous HP-AgNW/TPU electrodes provided comparable signal quality to the gel electrodes The measured signal to noise ratio (SNR) of the ECG by the porous HP-AgNW/TPU electrodes was 7.0 dB, comparable to that measured by the gel electrodes, 7.1 dB. Under continuous wrist movement, motion artifacts were introduced to the signals measured using both the dry porous HP-AgNW/TPU electrodes and commercial gel electrodes (Figure S9). The SNR of the ECG measured by HP-AgNW/TPU electrode and gel electrodes under movement are 6.3 dB and 6.2 dB, respectively. The HP-AgNW/TPU electrodes showed similar motion artifacts when compared with gel electrodes. The HP-AgNW/TPU electrodes showed higher susceptibility to motion artifacts compared with gel electrodes. For EMG, the signals corresponding to the muscle contraction for different grip strengths can be clearly distinguished. Notably the signal of the porous HP-AgNW/TPU electrodes was weaker than that of the gel electrodes, which is due to the different positions of the two types of electrodes (placed simultaneously). The measured SNR of the EMG by the reported electrodes (24.9 dB) was comparable to that measured by the gel electrodes (25.9 dB). Compared to commercial Ag/AgCl gel electrodes, the porous HP-AgNW/TPU electrodes do not require the conductive gel, which mitigates the skin irritation caused by the gel and the signal degradation due to dehydration of the gel.<sup>3</sup> In view of the gas permeability demonstrated earlier, these experiments further illustrate the feasibility of the porous HP-AgNW/TPU electrodes for long-term, continuous health monitoring.

In addition to skin-mountable applications, the electrodes can be integrated with textiles. Here we demonstrate the application of wireless capacitive touch sensing for human-machine interfaces.

Figure 5a shows the diagram of a touch sensor based on the self-capacitance mode.<sup>33</sup> Self-capacitive touch sensors use a single electrode to measure the apparent capacitance between the electrode and the virtual ground. Upon touched, the human-body capacitance is added to the self-capacitance circuit. As a result, the "touch" state can be determined by measuring the capacitance change. The capacitive breakout (MPR121 board) normalizes the capacitance into a "capacitance touch value", <sup>34</sup> which can be compared with a threshold value (*e.g.*, 40, as defined in this experiment) to identify the touch state. For example, if the value is lower than the threshold value, the electrode is being touched. Figure 5b shows the capacitance touch value from the capacitive breakout. It is seen that finger "touch" (*i.e.*, tap and press) can be clearly identified.

In addition, the sensitivity of the touch sensor system is defined as change rate of the reading value when a touch occurs,  $Sensitivity = \frac{V_n - V_t}{V_n} \times 100\%$ , where  $V_n$  is the non-trigger reading value and  $V_t$  is the trigger reading value. In our system, the sensitivity is calculated to be about 86%. The stability is defined as the dispersion of the touch sensor reading, which is about 1.65. The SNR of the system is about 35:1, and the response time is less than 0.1 s (Figure S11). These system parameters attest that our capacitance touch sensor system performs well for detecting finger touch.<sup>35</sup>

To assemble a wireless touch sensor system (Figure 5c), a piece of 50 mm × 100 mm HP-AgNW/TPU film was integrated onto a fabric sleeve and patterned into four touch sensors/keys using laser cutting.<sup>24</sup> Each key was connected to a port of the touch sensor breakout, and the touch sensor breakout was connected to the Bluetooth controller (Feather 32u4) and battery to complete the assembly of the system. These four keys were assigned with four functions: left, down, rotation, and right. Each function can be activated when the finger touches the corresponding key.

Then the sleeve was put on the arm and used as a wireless human-machine interface to play Tetris on a computer display (Movie S3). The system was set as a Bluetooth keyboard in the computer. Figure 5d shows the function of different keys and the movement trace of the tiles controlled by touching the keys. Upon pressing the keys of rotation, left, right and down on the sleeve, the tiles in the game produced corresponding real-time responses without noticeable delay. As illustrated in the video, the touch sensor was highly sensitive and accurate.

## **CONCLUSION**

Here we report facile fabrication of gas permeable, ultrathin, stretchable, semi-transparent and laser patternable electrodes for epidermal wearable applications, either directly mounted on skin or integrated with textiles. The porous structure was enabled by a self-assembly process using the breath figure method, and the electric conductance was made possible by dip-coating AgNWs on the skeleton of the porous structure. The pore morphology and ratio of through-pores can be controlled by the concentration of solution in the breath figure process. With an optimal concentration of 1.5 wt% TPU + 0.15 wt% PEG, through pores with size of around 40  $\mu m$  was achieved. After heat press post-treatment, AgNWs were embedded below the surface of TPU, which improved the adhesion between AgNWs and TPU and conductivity of the film, while maintaining good transmittance and water vapor permeability. Vapor permeability is critical for the evaporation of sweat, which can effectively prevent adverse effects on the skin. The resistance of the film can be programmed by the first stretch and stabilized in the subsequent stretch-release cycles. The film was conductive on the top and bottom surfaces as well as through thickness. With a thickness of only a few micrometers and the porous structure, the electrode enabled a conformal contact with skin, leading to low electrode-skin impedance and excellent ECG and EMG signals

on par with commercial gel electrodes. In the capacitive sensing application, the electrode was capable of responding to finger touches in real time with high accuracy. With unusual combination of the features including ultra-low thickness, semi-transparency, stretchability, gas permeability, facile fabrication, and laser patterning capability, the reported electrode offers a way for long-term wearable health monitoring and human-machine interfaces.

## **METHODS**

TPU film was purchased from Perfectex Plus LLC (Hot Melt Adhesive film model number #HM67-PA). PEG (average molecule weight 200) and THF were purchased from Fisher Scientific Reagent and used without further purification. AgNWs were synthesized using the polyol method.<sup>36, 37</sup> Deionized water was purified using a Milli-Q system (MilliporeSigma).

Fabrication of porous TPU film on glass substrate. The porous film was fabricated by the breath figure method. <sup>22, 38</sup> 1.5 g TPU and 0.15 ml PEG were dissolved into 100 ml THF solution. Then 5 ml of the solution was uniformly coated on a glass substrate (100 mm×200 mm) using a Meyer bar. After the bar coating process, the glass substrate was placed into a chamber with high humidity (relative humidity (RH): 99%, temperature: 25 °C) immediately. At this time, moisture was firstly condensed on the substrate and then merged to form a water droplet array. After the organic solvent and water droplets were evaporated, a porous TPU film was formed on the substrate after about 10 minutes. To facilitate the detachment of the porous TPU film from the glass substrate, a plastic frame was pressed onto the porous TPU film with the help of a double-sided adhesive tape. This way the porous TPU film can be peeled off the substrate. Afterwards, the porous TPU film was washed with DI water and dried at room temperature.

Coating AgNWs onto the porous TPU film. AgNWs were coated onto the film using dip coating. It is known that TPU swells in ethanol, methanol, isopropyl alcohol and other organic solvent, so AgNWs were dispersed in water in this experiment. Since TPU film is hydrophobic, plasma treatment for 3 minutes was introduced to render the surface hydrophilic. Then the treated TPU film was immersed into the AgNW solution (1 mg/ ml) for 30 seconds and dried at 60 °C for 15 minutes. The coating and drying process was repeated several times to ensure sufficient AgNWs coated onto the porous TPU film.

Heat press and patterning the porous AgNW/TPU film into designed patterns. The AgNW/TPU film was placed in between two sheets of PTFE and subjected to heat press at 150 °C under a pressure of 3×105 Pa. After that, the heat pressed porous AgNW/TPU film (HP-AgNW/TPU) was fabricated. To pattern the porous HP-AgNW/TPU, the film was attached onto a PTFE film with the help of moisture generated by a humidifier. Then the film was cut into the designed pattern by a laser cutter (VLS6.60, Universal Laser Systems) with 0.1% power, 20% speed, and 1000 PPI. After removing the excessive material, porous HP-AgNW/TPU film with the designed pattern was fabricated.

Characterization. The microstructures of porous TPU, porous AgNW/TPU, and porous HP-AgNW/TPU films were characterized by scanning electron microscopy (SEM, FEI Quanta 3D FEG) and optical microscopy (ECLIPSE LV150N, Nikon). The transmittance of each film was measured using a UV-vis spectrophotometer (Cary 5000, Agilent). The resistance of each film was measured using a digital multimeter (34401A, Agilent). The water vapor transmission of each film was measured on a homemade test system based on ASTM E96 standard. The testing process is as follows: a 20 ml sized plastic bottle was filled with 15 ml distilled water, then sealed with a sample using a double-sided tape. The bottle was placed in a chamber with a temperature of 35 °C

and RH of  $40\% \pm 5\%$ . The mass of the bottle was measured every 10 hours. The water vapor transmission was calculated based on the mass change. The electrode-skin impedance was obtained by performing a frequency sweep over a pair of electrodes placed at a distance of 7 cm on the forearm. The reported electrodes and gel electrodes were placed in adjacent. The electrode-skin impedance was measured using a potentiostat (Reference 600, Gamry Instruments). Electrocardiogram (ECG) and electromyography (EMG) signals were obtained using an amplifier (PowerLab 4/26, ADInstruments) with a sampling rate of 1 kHz. The SNR of ECG and EMG signals for both reported dry and commercial gel electrodes were calculated using the following

equation,  $^{32}$   $^{SNR_{dB}} = 10 \log_{10}(\frac{A_{\text{signal}}}{A_{\text{noise}}})^2 = 20 \log_{10}(\frac{A_{\text{signal}}}{A_{\text{noise}}})$ , where  $^{A_{\text{signal}}}$  is the root mean square of the biopotential signals (*i.e.*, ECG or EMG signals in this study),  $^{A_{\text{noise}}}$  is the root mean square of the noise collected in the settling trials. The Bluetooth controller (Feather 32u4 Bluefruit LE) and capacitive touch sensor breakout (MPR121) were purchased from Adafruit.

## ASSOCIATED CONTENT

## **Supporting Information**

The Supporting Information is available free of charge on the ACS *via* the Internet at http://pubs.acs.org. Additional figure including optical image of porous TPU films; Cross-section SEM images of porous TPU film, porous AgNW/TPU film and porous HP-AgNW/TPU film; The stress-strain curves of porous TPU, porous AgNW/TPU and porous HP-AgNW / TPU film; Photographs of the electrodes on skin before and after peeling off the electrodes after wearing for 7 days; Photographs of the AgNW/TPU and HP-AgNW/TPU electrodes on skin before and after peeling off; Schematic and photograph of the LED circuit; Relative resistance changes during 1000

cycles of stretching and releasing with 10% tensile strain; Relative resistance change as a function

of tensile strain for the porous HP-AgNW/TPU film with larger strain; Optical image of the

patterned electrode transferred on a wrinkled artificial skin; ECG signals measured using the

commercial gel electrodes and porous HP-AgNW/TPU electrodes under continuous motion;

Capacitive touch value changes versus time. Additional movies including lamination process of

the patterned porous HP-AgNW/TPU electrode (Movie S1); Removal process of the patterned

porous HP-AgNW/TPU electrode (Movie S2); Demo of playing game (Tetris) using the patterned

electrodes (Movie S3).

**AUTHOR INFORMATION** 

**Corresponding Authors** 

\*E-mail: yong zhu@ncsu.edu or iamywma@njupt.edu.cn

ACKNOWLEDGMENT

The authors gratefully acknowledge the financial support from the National Science Foundation

(NSF) through Award No. CMMI-1728370. W. Z. would like to thank the financial support from

NSFC (51772157), and Keypoint Research and Invention Program of Jiangsu Province

(BE2018010-3). We thank Prof. Chih-Hao Chang and Zhiren Luo for assistance with the

transmittance measurement.

REFERENCES

Chen, D.; Pei, Q., Electronic Muscles and Skins: A Review of Soft Sensors and Actuators. 1.

Chem. Rev. 2017, 117, 11239-11268.

16

- 2. Liu, Y.; He, K.; Chen, G.; Leow, W. R.; Chen, X., Nature-Inspired Structural Materials for Flexible Electronic Devices. *Chem. Rev.* **2017**, *117*, 12893-12941.
- 3. Yao, S.; Swetha, P.; Zhu, Y., Nanomaterial-Enabled Wearable Sensors for Healthcare. *Adv. Healthcare Mater.* **2018,** *7*, 1700889.
- 4. Kim, D. H.; Ghaffari, R.; Lu, N.; Rogers, J. A., Flexible and Stretchable Electronics for Biointegrated Devices. *Annu. Rev. Biomed. Eng.* **2012**, *14*, 113-128.
- 5. Yao, S.; Ren, P.; Song, R.; Liu, Y.; Huang, Q.; Dong, J.; O'Connor, B. T.; Zhu, Y., Nanomaterial-Enabled Flexible and Stretchable Sensing Systems: Processing, Integration, and Applications. *Adv. Mater.* **2019**, e1902343.
- 6. Kim, D. H.; Lu, N.; Ma, R.; Kim, Y. S.; Kim, R. H.; Wang, S.; Wu, J.; Won, S. M.; Tao, H.; Islam, A.; Yu, K. J.; Kim, T. I.; Chowdhury, R.; Ying, M.; Xu, L.; Li, M.; Chung, H. J.; Keum, H.; McCormick, M.; Liu, P., *et al.*, Epidermal Electronics. *Science* **2011**, *333*, 838-843.
- 7. Trung, T. Q.; Lee, N. E., Flexible and Stretchable Physical Sensor Integrated Platforms for Wearable Human-Activity Monitoring and Personal Healthcare. *Adv. Mater.* **2016**, *28*, 4338-4372.
- 8. Kaltenbrunner, M.; Sekitani, T.; Reeder, J.; Yokota, T.; Kuribara, K.; Tokuhara, T.; Drack, M.; Schwodiauer, R.; Graz, I.; Bauer-Gogonea, S.; Bauer, S.; Someya, T., An Ultra-Lightweight Design for Imperceptible Plastic Electronics. *Nature* **2013**, *499*, 458-463.
- 9. Lipomi, D. J.; Vosgueritchian, M.; Tee, B. C.; Hellstrom, S. L.; Lee, J. A.; Fox, C. H.; Bao, Z., Skin-Like Pressure and Strain Sensors Based on Transparent Elastic Films of Carbon Nanotubes. *Nat. Nanotechnol.* **2011**, *6*, 788-792.
- 10. Yeo, W. H.; Kim, Y. S.; Lee, J.; Ameen, A.; Shi, L.; Li, M.; Wang, S.; Ma, R.; Jin, S. H.; Kang, Z.; Huang, Y.; Rogers, J. A., Multifunctional Epidermal Electronics Printed Directly onto the Skin. *Adv. Mater.* **2013**, *25*, 2773-2778.

- 11. Gong, S.; Yap, L. W.; Zhu, B.; Cheng, W., Multiscale Soft–Hard Interface Design for Flexible Hybrid Electronics. *Adv. Mater.* **2019**, 1902278.
- 12. Kim, H. W.; Kim, T. Y.; Park, H. K.; You, I.; Kwak, J.; Kim, J. C.; Hwang, H.; Kim, H. S.; Jeong, U., Hygroscopic Auxetic On-Skin Sensors for Easy-To-Handle Repeated Daily Use. *ACS Appl. Mater. Interfaces* **2018**, *10*, 40141-40148.
- 13. Yang, S.; Chen, Y. C.; Nicolini, L.; Pasupathy, P.; Sacks, J.; Su, B.; Yang, R.; Sanchez, D.; Chang, Y. F.; Wang, P.; Schnyer, D.; Neikirk, D.; Lu, N., "Cut-And-Paste" Manufacture of Multiparametric Epidermal Sensor Systems. *Adv. Mater.* **2015**, *27*, 6423-6430.
- 14. Kim, J. H.; Kim, S. R.; Kil, H. J.; Kim, Y. C.; Park, J. W., Highly Conformable, Transparent Electrodes for Epidermal Electronics. *Nano Lett.* **2018**, *18*, 4531-4540.
- 15. You, I.; Kim, B.; Park, J.; Koh, K.; Shin, S.; Jung, S.; Jeong, U., Stretchable E-Skin Apexcardiogram Sensor. *Adv. Mater.* **2016**, *28*, 6359-6364.
- 16. Gong, S.; Yap, L. W.; Zhu, B.; Zhai, Q.; Liu, Y.; Lyu, Q.; Wang, K.; Yang, M.; Ling, Y.; Lai, D. T. H.; Marzbanrad, F.; Cheng, W., Local Crack-Programmed Gold Nanowire Electronic Skin Tattoos for In-Plane Multisensor Integration. *Adv. Mater.* **2019**, *31*, e1903789.
- 17. Miyamoto, A.; Lee, S.; Cooray, N. F.; Lee, S.; Mori, M.; Matsuhisa, N.; Jin, H.; Yoda, L.; Yokota, T.; Itoh, A.; Sekino, M.; Kawasaki, H.; Ebihara, T.; Amagai, M.; Someya, T., Inflammation-Free, Gas-Permeable, Lightweight, Stretchable On-Skin Electronics with Nanomeshes. *Nat. Nanotechnol.* **2017**, *12*, 907-913.
- 18. Sun, B.; McCay, R. N.; Goswami, S.; Xu, Y.; Zhang, C.; Ling, Y.; Lin, J.; Yan, Z., Gas-Permeable, Multifunctional On-Skin Electronics Based on Laser-Induced Porous Graphene and Sugar-Templated Elastomer Sponges. *Adv. Mater.* **2018**, *30*, e1804327.

- 19. Fan, Y. J.; Li, X.; Kuang, S. Y.; Zhang, L.; Chen, Y. H.; Liu, L.; Zhang, K.; Ma, S. W.; Liang, F.; Wu, T.; Wang, Z. L.; Zhu, G., Highly Robust, Transparent, and Breathable Epidermal Electrode. *ACS Nano* **2018**, *12*, 9326-9332.
- 20. Cai, L.; Song, A. Y.; Wu, P.; Hsu, P. C.; Peng, Y.; Chen, J.; Liu, C.; Catrysse, P. B.; Liu, Y.; Yang, A.; Zhou, C.; Zhou, C.; Fan, S.; Cui, Y., Warming Up Human Body by Nanoporous Metallized Polyethylene Textile. *Nat. Commun.* **2017**, *8*, 496.
- 21. Bai, H.; Du, C.; Zhang, A.; Li, L., Breath Figure Arrays: Unconventional Fabrications, Functionalizations, and Applications. *Angew. Chem. Int. Ed. Engl.* **2013**, *52*, 12240-12255.
- 22. Zhang, A.; Bai, H.; Li, L., Breath Figure: A Nature-Inspired Preparation Method for Ordered Porous Films. *Chem. Rev.* **2015**, *115*, 9801-9868.
- 23. Ponnusamy, T.; Lawson, L. B.; Freytag, L. C.; Blake, D. A.; Ayyala, R. S.; John, V. T., *In Vitro* Degradation and Release Characteristics of Spin Coated Thin Films of PLGA with a "Breath Figure" Morphology. *Biomatter* **2012**, *2*, 77-86.
- 24. Yao, S.; Yang, J.; Poblete, F. R.; Hu, X.; Zhu, Y., Multifunctional Electronic Textiles Using Silver Nanowire Composites. *ACS Appl. Mater. Interfaces* **2019**, *11*, 31028-31037.
- 25. Cui, Z.; Poblete, F. R.; Zhu, Y., Tailoring the Temperature Coefficient of Resistance of Silver Nanowire Nanocomposites and Their Application as Stretchable Temperature Sensors. *ACS Appl. Mater. Interfaces* **2019**, *11*, 17836-17842.
- 26. Standard Test Methods for Water Vapor Transmission of Materials. ASTM International: West Conshohocken, PA, 2016. 1-12.
- 27. Xu, F.; Wang, X.; Zhu, Y.; Zhu, Y., Wavy Ribbons of Carbon Nanotubes for Stretchable Conductors. *Adv. Funct. Mater.* **2012,** *22*, 1279-1283.

- 28. Zhu, Y.; Xu, F., Buckling of Aligned Carbon Nanotubes as Stretchable Conductors: A New Manufacturing Strategy. *Adv. Mater.* **2012**, *24*, 1073-1077.
- 29. Xu, F.; Zhu, Y., Highly Conductive and Stretchable Silver Nanowire Conductors. *Adv. Mater.* **2012,** *24*, 5117-5122.
- 30. Yao, S.; Zhu, Y., Nanomaterial-Enabled Stretchable Conductors: Strategies, Materials and Devices. *Adv. Mater.* **2015,** *27*, 1480-1511.
- 31. Jin, L.; Chortos, A.; Lian, F.; Pop, E.; Linder, C.; Bao, Z.; Cai, W., Microstructural Origin of Resistance-Strain Hysteresis in Carbon Nanotube Thin Film Conductors. *Proc. Natl. Acad. Sci.* **2018**, *115*, 1986-1991.
- 32. Myers, A. C.; Huang, H.; Zhu, Y., Wearable Silver Nanowire Dry Electrodes for Electrophysiological Sensing. *RSC Adv.* **2015**, *5*, 11627-11632.
- 33. Barrett, G.; Omote, R., Projected-Capacitive Touch Technology. *Inf. Disp.* **2010**, *26*, 16-21.
- 34. Nelson, C. Hello Capacitive Touch. https://learn.adafruit.com/circuit-playground-fruit-drums/hello-capacitive-touch (accessed April 15, 2020).
- 35. Touch Sensor Application Note. https://github.com/espressif/esp-iot-solution/blob/master/documents/touch\_pad\_solution/touch\_sensor\_design\_en.md (accessed April 15, 2020).
- 36. Sun, Y.; Xia, Y., Large-Scale Synthesis of Uniform Silver Nanowires through a Soft, Self-Seeding, Polyol Process. *Adv. Mater.* **2002**, *14*, 833-837.
- 37. Zhu, Y.; Qin, Q.; Xu, F.; Fan, F.; Ding, Y.; Zhang, T.; Wiley, B. J.; Wang, Z. L., Size Effects on Elasticity, Yielding, and Fracture of Silver Nanowires: *In Situ* Experiments. *Phys. Rev. B: Condens. Matter* **2012**, *85*, 045443.

38. Wan, L. S.; Ke, B. B.; Zhang, J.; Xu, Z. K., Pore Shape of Honeycomb-Patterned Films: Modulation and Interfacial Behavior. *J. Phys. Chem. B* **2012**, *116*, 40-47.

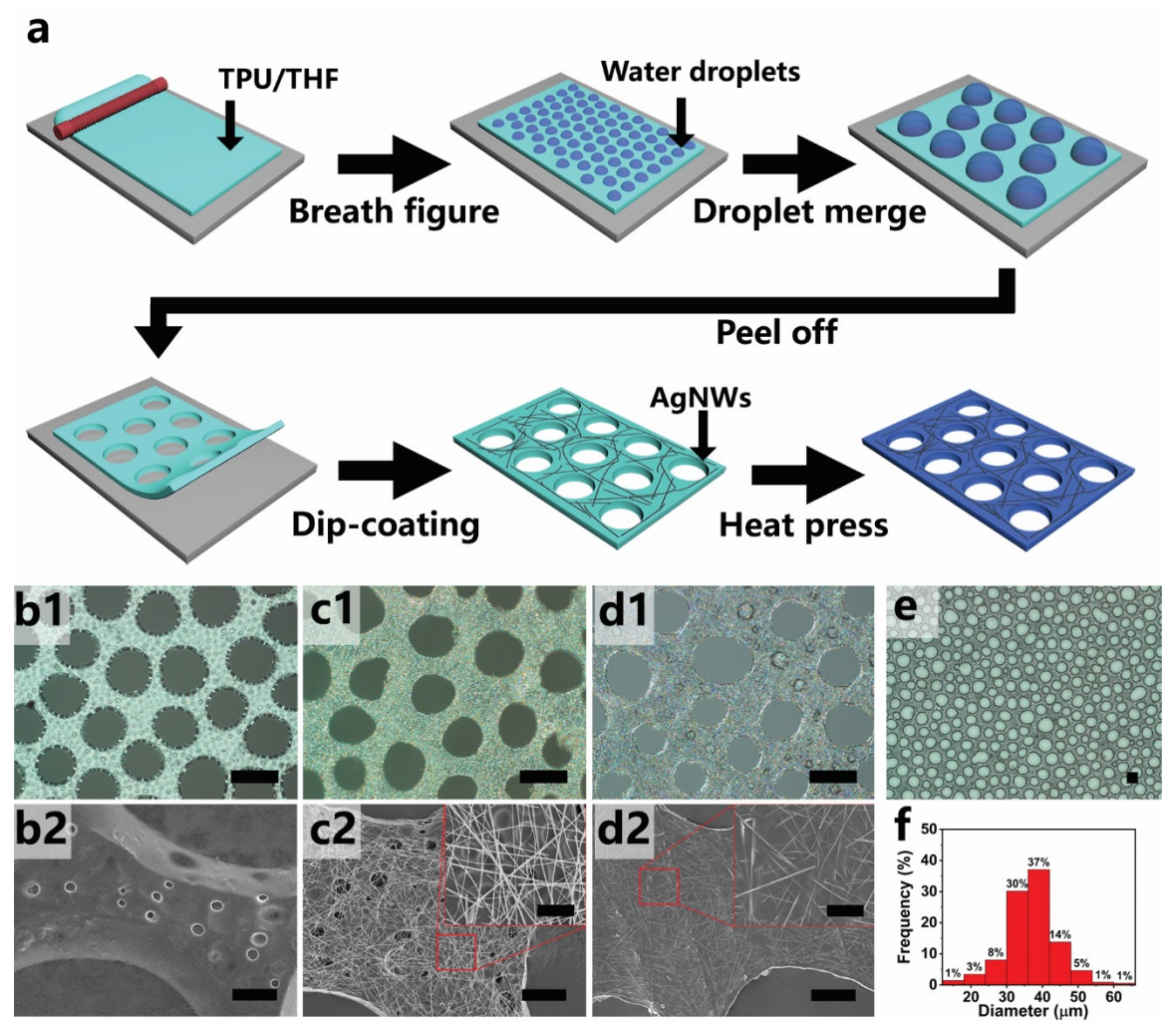


**Figure 1.** (a) Schematic illustration of the fabrication process for porous HP-AgNW/TPU film. Optical (top) and SEM (bottom) images of: (b1, b2) porous TPU film; (c1, c2) porous AgNW/TPU film; (d1, d2) porous HP-AgNW/TPU film. e) Optical image of porous TPU film. f) The pore size distribution. Scale bars: 40  $\mu$ m in optical images, 20  $\mu$ m in SEM images, and 5  $\mu$ m in the insert images in c2 and d2.

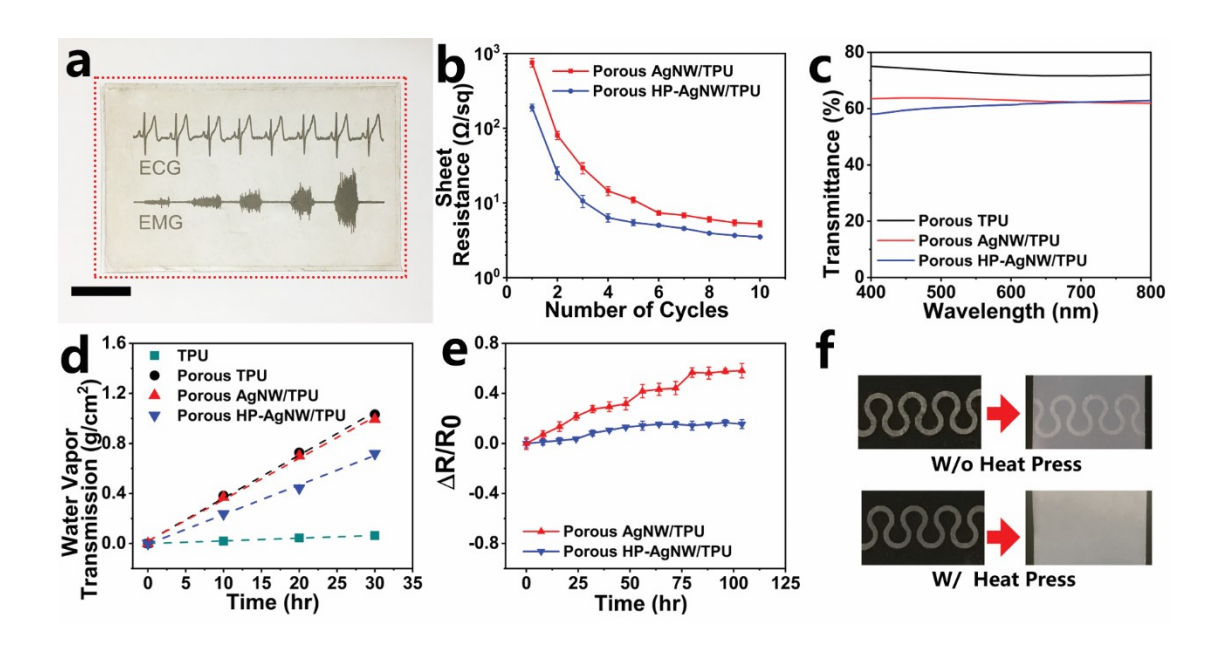


Figure 2. (a) Photograph of the porous HP-AgNW/TPU film showing good optical transmittance. The dotted lines show the boundary of the film. Scale bars, 40 mm (b) Sheet resistance as a function of number of dip-coating cycles. (c) Transmittance spectrum of the porous TPU, AgNW/TPU and HP-AgNW/TPU films. (d) Water vapor transmission of the porous TPU, AgNW/TPU and HP-AgNW/TPU films as a function of time. (e) Relative resistance change when the porous AgNW/TPU and HP-AgNW/TPU films were immersed in saline solution. (f) Photograph of the porous AgNW/TPU and HP-AgNW/TPU films after the peeling test on tape.

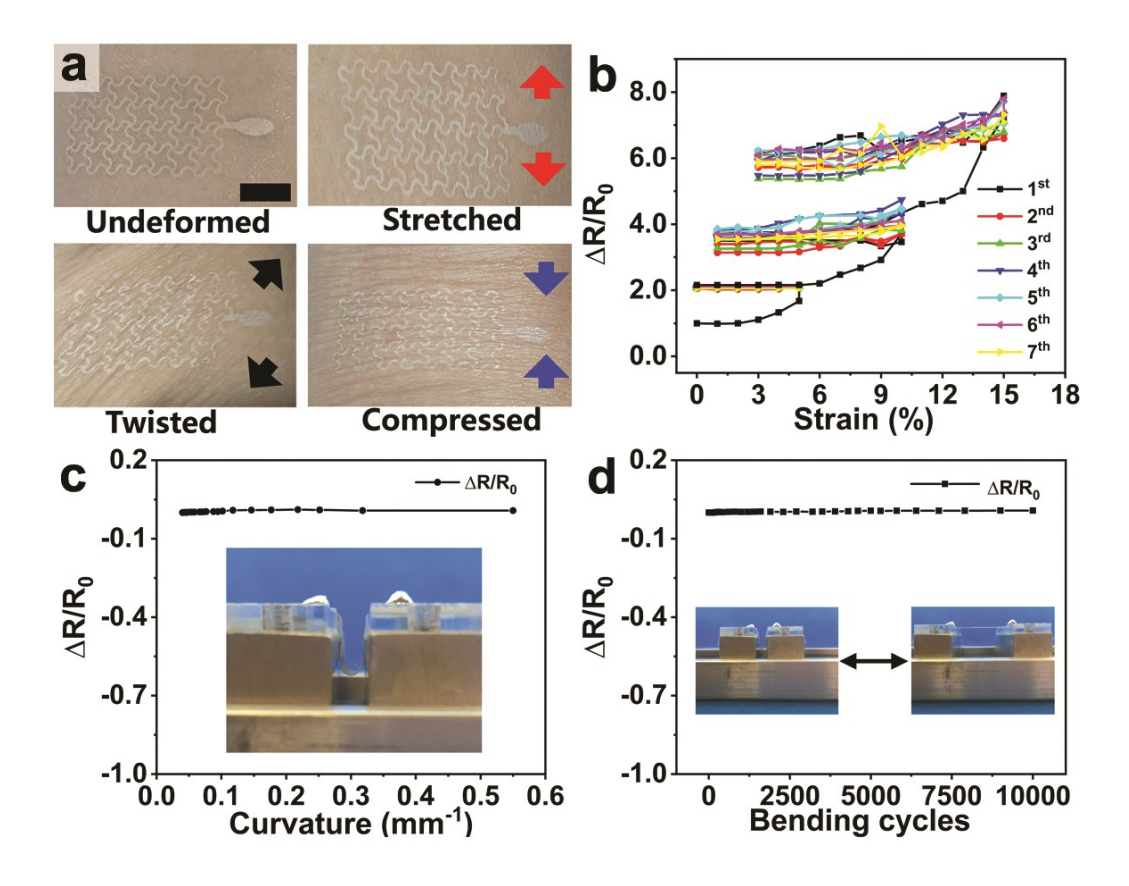
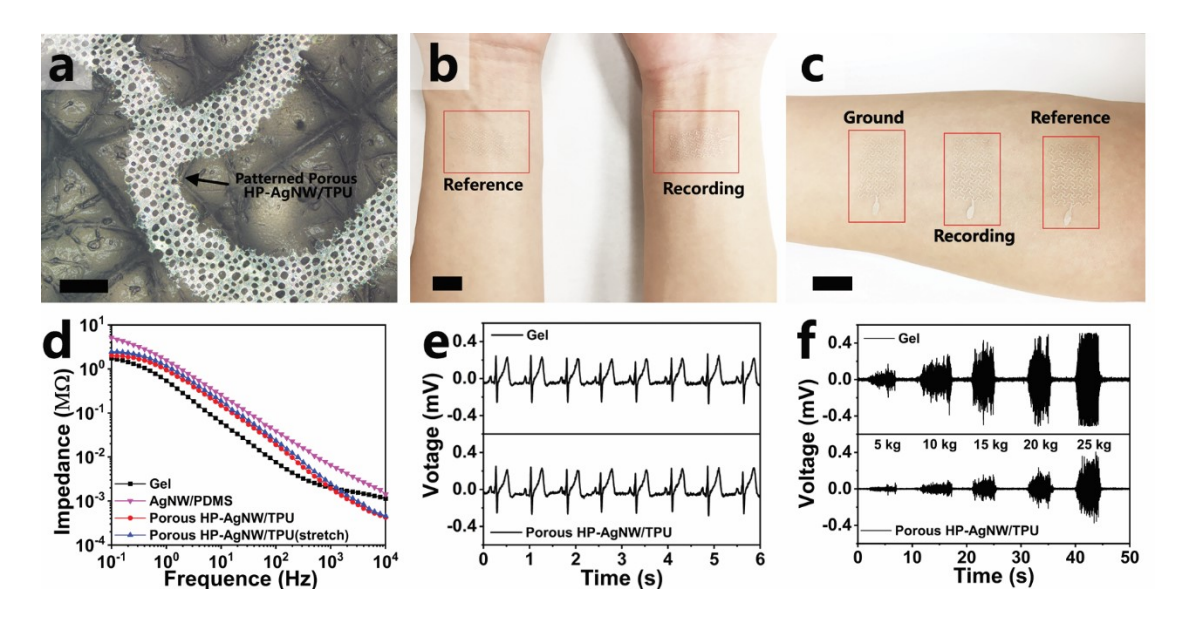
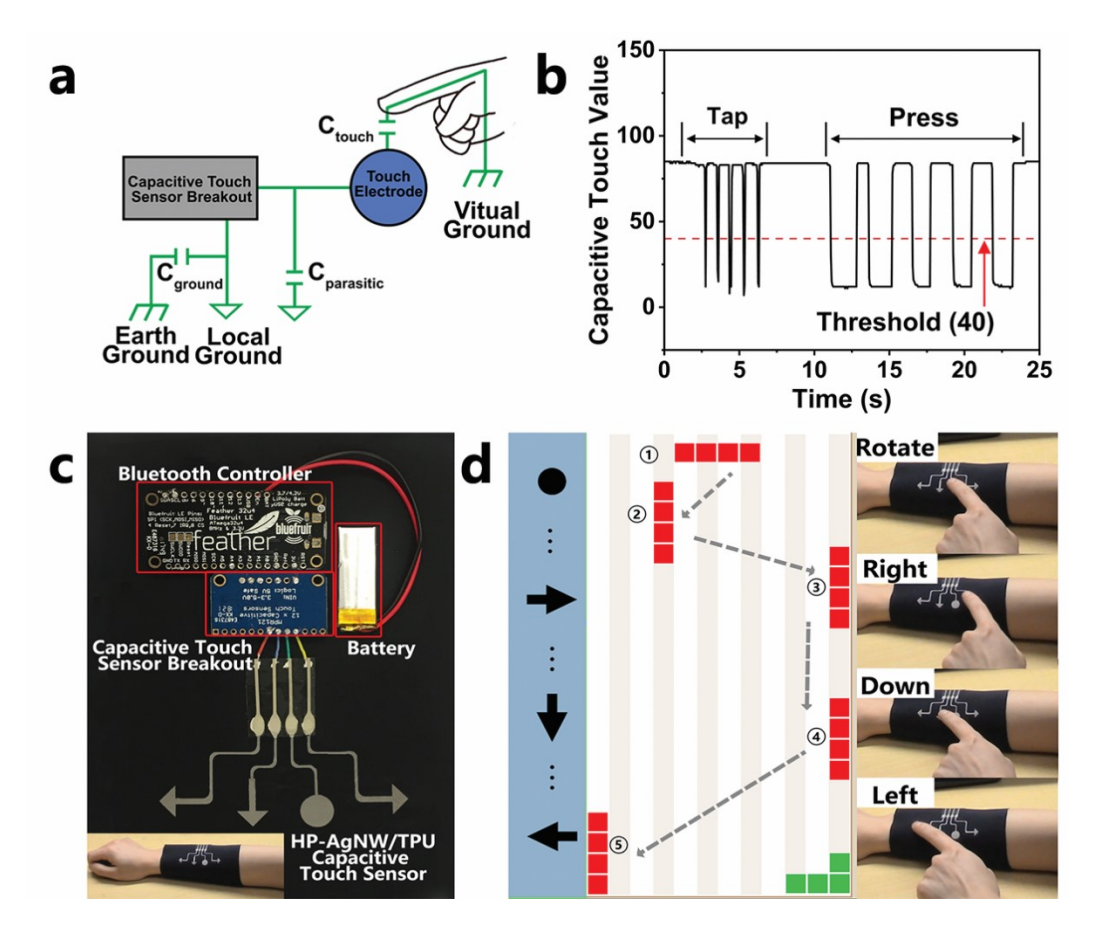


Figure 3. (a) Top view of an electrophysiological electrode on skin (top left). Scale bar, 5 mm. The image shown the EP electrode on skin when stretched (top right), compressed (bottom right) and twisted (bottom left). (b) Relative resistance change as a function of tensile strain for the porous HP-AgNW/TPU film. 7 cycles of stretching and releasing were applied at each strain level. c,d) Relative resistance change when the porous HP-AgNW/TPU film was subjected to bending (c) and cyclic bending (d), respectively.



**Figure 4.** Application of the electrode in electrophysiological sensing. (a) Optical image of the electrode transferred on the artificial skin. Scale bars, 400 μm in optical image (b) Photograph of the porous HP-AgNW/TPU electrodes attached onto left and right forearms for ECG testing. (c) Photograph of three porous HP-AgNW/TPU electrodes attached onto the forearm for EMG testing. Scale bars, 10 mm in digital photograph (d) Electrode-skin impedance of commercial gel electrodes, AgNW/PDMS electrodes, porous AgNW/TPU electrodes, and porous HP-AgNW/TPU electrodes. (e) ECG signals measured using the commercial gel electrodes and porous HP-AgNW/TPU electrodes placed nearby. (f) EMG signals measured using the commercial gel electrodes and porous HP-AgNW/TPU electrodes placed nearby. The grip strength was measured by a hand dynamometer.



**Figure 5.** Application of the electrode in wireless human-computer interface. (a) Schematic diagram of the touch sensor based on the self-capacitance mode. The C<sub>parasitic</sub> is the basic capacitance of the touch sensor system. (b) Capacitive touch values from the capacitive breakout. (c) Layout of the wireless human-computer interface with the porous HP-AgNW/TPU patterns as touch sensors. The insert on the bottom left shows the sleeve worn on the arm. (d) Application in playing Tetris. The four keys correspond to four different functions: moving left, moving down, rotating, and moving right, respectively.

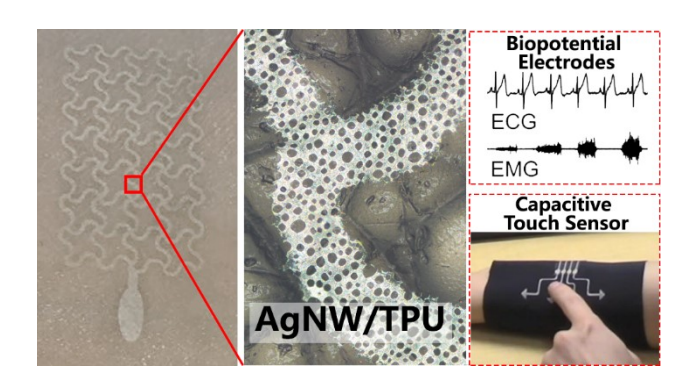


Table of Content (TOC) Graphic